Amplitude equations for extended discrete systems: A study of an antiferromagnetic spin chain

B. Rumpf* and H. Sauermann
Institut für Festkörperphysik, Darmstadt University of Technology, Hochschulstrasse 8, 64289 Darmstadt, Germany
(Received 16 June 1997; revised manuscript received 27 April 1998)

We study the effect of the dynamical degrees of freedom resulting from the lattice structure of an antiferromagnet on pattern forming bifurcations. They are examined in a one-dimensional chain of damped and driven classical spin oscillators. In addition to stationary states where all spins are parallel (quasiferromagnetic state), it exhibits states where the spins are lined up on two sublattices (noncollinear state). Besides showing instabilities against large scale perturbations, short wavelengths of the order of the lattice constant become critical even for weak driving fields. A general formalism admitting a dynamical description of discrete oscillator chains in the weakly nonlinear regime beyond the instabilities is developed. The ensuing amplitude equation allows the examination of the formation of patterns in this domain. Special emphasis is laid on instabilities of higher codimension. A codimension-3 bifurcation where all wave numbers become critical simultaneously implies a direct transition to turbulence. [S1063-651X(98)04608-X]

PACS number(s): 05.50.+q, 75.10.Hk, 02.30.Mv

I. INTRODUCTION

Numerous experimental and theoretical investigations of the ferromagnetic response to time dependent external fields have made driven magnets a paradigm of nonlinear science. Following the observation by Bloembergen, Damon, and Wang [1] of broadened power absorption spectra of ferrit samples strongly driven by microwaves, theoretical treatments [2] have explained the emergence of a new state characterized by pairs of spin waves above a first instability threshold. Experimentally observed auto-oscillations have been interpreted as limit cycles emanating from a secondary Hopf bifurcation of this state. Driving fields well above this threshold have led to intricate bifurcation phenomena including a period doubling route to chaos that has been reproduced in idealized model systems [3]. In detecting the response of the whole sample and not resolving spatial patterns, such experiments are restricted to temporal dynamics.

Empirical and formal similarities of driven magnetic systems to fluids suggest the occurrence of turbulent states [4] and long scale patterns [5,6] in the magnetization. Fundamental theoretical studies taking the nonlocal dipolar term into account even predict pattern switching phenomena in ferromagnetic films [7].

But unlike fluids or liquid crystals, magnetism has not yet become representative for nonequilibrium pattern formation. The reason for this seems to be twofold: firstly, available driving field strengths require samples with relatively small linewidths. In this case, the complex Ginzburg-Landau equation typically obtained by perturbation theoretic expansions is valid on extremely long time scales; beyond a small region above threshold it may be studied in the limit of the nonlinear Schrödinger equation. Consequently, weakly damped systems are frequently approximated by Hamiltonian descriptions; such systems have been examined in thermodynamics and the investigation of solitons [8–10]. Secondly, a major obstacle lies in the experimentally difficult resolution of small variations of the magnetization in spatiotemporal patterns, using, e.g., the Faraday effect in thin ferrimagnetic films. This method is well established [10] to visualize domain structures, moving domain walls or solitons where the considerable changes of the magnetization cause observable rotations of the polarization of light. Also precession angles in ferrimagnetic resonance were measured [11]. However, to our knowledge visualizing the slow variations of an envelope characteristic for dissipative pattern formation has not yet been achieved. Rapid pattern switching in two dimensions might also impede the observation.

Still, in strongly driven magnets nonequilibrium pattern formation should be observable; both the Faraday effect and the linewidth are enhanced by an appropriate dotting, which seems to be a promising way to observe one and two dimensional patterns in thin magnetic films.

In formal descriptions, simplifications of the complex mechanisms present in real magnets are indispensable. Theoretical approaches are based, e.g., on the S theory or the Landau-Lifshitz equation. Even though the microscopic description of magnetism is purely quantum mechanical, macroscopic dynamical properties are described appropriately by classical equations of motion. The Landau-Lifshitz equation was originally a purely phenomenological description of the dynamics of the magnetization density of a ferromagnet; now, somewhat in analogy to Navier-Stokes in fluid mechanics, there are sound microscopic derivations [12] including assessments of its applicability.

For systems consisting of two or more [13] sublattices such as antiferromagnets and weak ferromagnets [10], the situation is even more complicated. Each sublattice may be described separately by a classical Landau-Lifshitz equation [14]. The effective field at each lattice site contains a coupling term to the nearest neighbors on the other sublattice. The nonlocal dipolar term may be neglected if the resulting magnetization is weak.

Microscopically, discrete models appear to be the most adequate description for antiferromagnetism of ionic crystals

*FAX: +49 6151 16 4165. Electronic address: benno@arnold.fkp.physik.th-darmstadt.de

with localized atomic momenta. Even then, working from the assumption that neighboring spins are approximately in the same state, a continuum transition is often performed in the Hamiltonian [8,9] or in the primary Landau-Lifshitz equation [15–18]. This assumption breaks down if there are short wavelength excitations. We will show that this can be the case for damped and driven systems. We describe our system as a set of coupled ordinary differential equations, thus taking the discreteness effects into account.

We formulate a model system that includes the basic physical features of driven antiferromagnets, but is still simple enough to admit analytical studies pattern formation mechanisms. The dynamics is restricted to one spatial dimension reflecting a strongly anisotropic exchange interaction in the crystal. The emphasis is put on bifurcational studies in a wide range of parameter space that may serve as a guide for studies specified to particular materials.

To understand spatiotemporal dynamics near an instability threshold, a systematic reduction of the degrees of freedom is often more helpful than the computation of particular solutions. This reduction transforms the original equation of motion to a canonic amplitude equation, whose form is determined entirely by the type of instability under consideration. The coefficients of the reduced equation are functions of the original physical parameters. Different physical systems may therefore be treated in a unifying manner. Such reductions are well established as center manifold reductions in low dimensional systems [19] and as solvability conditions within a multiple scale perturbation theory of partial differential equations for spatially extended systems [20].

While our system itself is discrete, its slowly varying amplitude admits a description by partial differential equations. We present a derivation of amplitude equations for quite general chains of coupled oscillators. Applying this formalism to the magnetic system yields all the parameters of the ensuing Ginzburg-Landau equation, which is well studied in the field of pattern formation [21]. This analysis provides a nonlinear characterization of the dynamics beyond the instabilities. Our formulas for the coefficients of the amplitude equation can be easily used for all locally coupled oscillator chains elucidating some universal aspects of magnetic pattern formation.

The one dimensional spin chain described in Sec. II contains a Landau-Lifshitz damping term and a rotating driving field. Bifurcations of the quasiferromagnetic state are studied in Sec. III. Noncollinear stationary states, in which the magnetization vectors of both sublattices deviate from the antiparallel alignment, are computed in Appendix A. Their most interesting instability represents a splitting of one sublattice into two sublattices, each of which can be described by a smooth function. The corresponding bifurcation scenario is studied in Sec. IV. In Appendix B the loci of these bifurcations in parameter space are determined explicitly for weak damping. The survey of the dynamics beyond the instabilities is carried out in Sec. V with the help of the general amplitude equation formalism presented in Appendix C. For the application to the antiferromagetic spin chain, the formalism is generalized to chains of two alternating types of oscillators. This is done in a parity-preserving way, which is developed from a discussion of frequently used continuum approximations of antiferromagnets (Appendix D). A bifurcation where all wavelengths become critical engendering turbulent motion is discussed in Sec. VI.

II. THE SYSTEM

As a model of a microwave-driven one-dimensional antiferromagnet we study a one-dimensional lattice of coupled classical spin oscillators $\mathbf{S}_n$ governed by the dissipative Landau-Lifshitz equation:

$$-\dot{\mathbf{S}}_n=\mathbf{S}_n\times\mathbf{H}_n+\Gamma\mathbf{S}_n\times(\mathbf{S}_n\times\mathbf{H}_n) \tag{1}$$

under the influence of the effective field

$$\mathbf{H}_n=B_0(\mathbf{e}_x\cos\,\omega t+\mathbf{e}_y\sin\,\omega t)+B_z\mathbf{e}_z+J(\mathbf{S}_{n-1}+\mathbf{S}_{n+1})\,. \tag{2}$$

$\mathbf{S}$ is a three dimensional real vector. The equation of motion conserves the modulus of $\mathbf{S}$; we set $|\mathbf{S}|=1$. Classical spins may be viewed as averaged magnetic momenta of several quantum mechanical spins, e.g., the spins of a sublattice in an antiferromagnet or the spins of a film in a superlattice [22]. The lattice-structure of the crystal is reflected in the discreteness of the chain. This admits to describe the spontaneous formation of sublattices in a uniform system.

The system is driven by a time dependent field B_0 rotating perpendicularly to the stationary external field B_z. $J<0$ is the antiferromagnetic Heisenberg exchange constant. Γ is the coefficient of the Landau-Lifshitz damping term. All these parameters are real.

The explicit time dependence can be eliminated by introducing a rotating coordinate system $\mathbf{e}'_x=\mathbf{e}_x\cos\,\omega t+\mathbf{e}_y\sin\,\omega t, \mathbf{e}'_y=-\mathbf{e}_x\sin\,\omega t+\mathbf{e}_y\cos\,\omega t, \mathbf{e}'_z=\mathbf{e}_z$. It leads to

$$-\dot{\mathbf{S}}_n=\mathbf{S}_n\times(\mathbf{H}_n-\omega\mathbf{e}_z)+\Gamma\mathbf{S}_n\times(\mathbf{S}_n\times\mathbf{H}_n) \tag{3}$$

with

$$\mathbf{H}_n=B_0\mathbf{e}_x+B_z\mathbf{e}_z+J(\mathbf{S}_{n-1}+\mathbf{S}_{n+1}). \tag{4}$$

Making use of the conservation of modulus to reduce the number of field equations and applying the stereographic projection into the complex plane $z=(S_x+iS_y)/(1+S_z)$ we obtain the equation of motion for the oscillator with index n

$$\begin{aligned}\dot{z}_n=&(i-\Gamma)B_z z_n-i\omega z_n-(i-\Gamma)\frac{B_0}{2}(1-z_n^2)\\&+J(i-\Gamma)(z_n-z_{n+1})\frac{1+z_n z^*_{n+1}}{1+z_{n+1}z^*_{n+1}}\\&+J(i-\Gamma)(z_n-z_{n-1})\frac{1+z_n z^*_{n-1}}{1+z_{n-1}z^*_{n-1}}.\end{aligned} \tag{5}$$

The system has states where the spins are arranged in one or two sublattices. In the following sections we will discuss their bifurcation scenario.

III. BIFURCATIONS OF THE QUASIFERROMAGNETIC STATE

A stationary state where all spins are parallel ($\mathbf{S}_n=\mathbf{S}_m$ for all n,m) is called a quasiferromagnetic state. In this case the Heisenberg coupling term $\mathbf{S}_n\times\mathbf{S}_{n+1}$ is identically zero and consequently such states are just the stationary solutions of the equation of motion of a single spin

$$\dot{z}=(i-\Gamma)B_z z-i\omega z-(i-\Gamma)\frac{B_0}{2}(1-z^2). \tag{6}$$

There are two such states

$$z_{A/B}=-\frac{(i-\Gamma)B_z-i\omega+\xi_{A/B}}{(i-\Gamma)B_0}, \tag{7}$$

where we have used the abbreviation

$$\xi_{A/B}=\pm\sqrt{[(i-\Gamma)B_z-i\omega]^2+[(i-\Gamma)B_0]^2}. \tag{8}$$

The root is defined so that Re $\xi_A\geqslant 0$,Re $\xi_B\leqslant 0$. We will now discuss instabilities of these solutions. The eigenvalues of a linear stability analysis are

$$\lambda_{A/B1}(k)=\xi_{A/B}+2J(i-\Gamma)(1-\cos k), \tag{9}$$

$$\lambda_{A/B2}(k)=\overline{\lambda}_{A/B1}(k). \tag{10}$$

k is the wave vector of the perturbations. The fixed point A is always unstable, while the fixed point B can be stable or unstable. The real part of the eigenvalues has extrema at $k=0$ and $k=\pi$. For antiferromagnetic coupling $J<0$ the real part of the eigenvalues, Re $\lambda_B(k)$, is maximal at $k=\pi$ and there is a wave instability when

$$\text{Re }\lambda_B(\pi)=\text{Re }\xi_B-4J\Gamma=0 \tag{11}$$

if Im $\xi_B+4J\neq 0$. This bifurcation takes place at the boundary of the Brillouin zone and can be regarded as a Hopf bifurcation of a related 2-spin system [3]. Above this instability, the lattice splits up into two sublattices. Two neighboring spins are excited with opposite phases $\Delta\mathbf{S}_n=-\Delta\mathbf{S}_{n+1}$.

This bifurcation corresponds to line W_0 in Fig. 1. In region Σ_0 above line W_0 there is one stable and one unstable quasiferromagnetic state. The strong external field neutralizes the antiferromagnetic interaction and stabilizes the energetically unfavorable parallel orientation. Below W_0, the antiferromagnetic interaction predominates and the quasiferromagnetic states are both unstable.

For $B_0^2=16J^2+\Gamma^2B_z^2$ and $\omega=(1+\Gamma^2)B_z$ the eigenvalues $\lambda_{1/2}$ vanish altogether (point a in Fig. 1). A nonlinear analysis of this bifurcation reveals saddle-node bifurcations of secondary fixed points [3] and also Hopf bifurcations and global bifurcations [23]. Instabilities of these noncollinear states far from this bifurcation will be studied in the next section.

IV. BIFURCATIONS OF NONCOLLINEAR STATES

Stationary solutions of Eq. (1) with the property

$$\mathbf{S}_{2n}=\mathbf{S}_A,\mathbf{S}_{2n+1}=\mathbf{S}_B \tag{12}$$

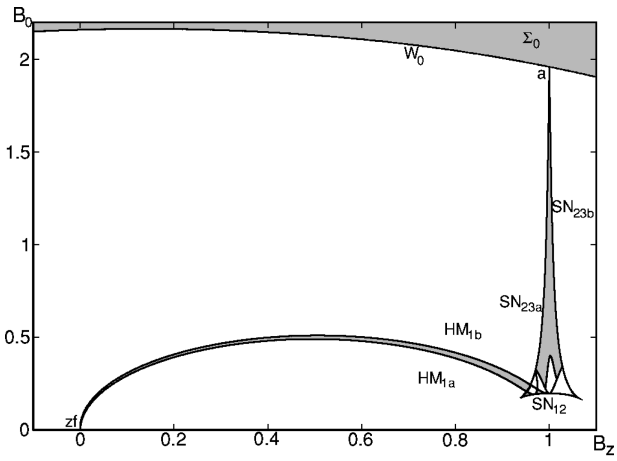

FIG. 1. Bifurcation scenario for $J=-0.49,\omega=1,\Gamma=0.01$. A trivial fixed point (all spins are parallel), which is stable in region Σ_0, becomes unstable at line W_0. Inside the triangular structure whose borders are saddle-node lines SN three nontrivial fixed points exist, outside there is only one. In the shaded areas, exactly one fixed point is stable.

for all n are called noncollinear states. They describe two homogeneously magnetized sublattices which are usually neither parallel nor antiparallel [Fig. 3(a)]. Such new 2-sublattice states are generated by the driving field. The canting is provoked by the driving field balancing the antiferromagnetic interaction. All these solutions can be determined exactly with the help of the third order polynomial

$$\Gamma^2\omega^2(1+m)^2(B_0^2-16J^2m)=[(1+\Gamma^2)B_0^2+(B_z-\omega)^2+\Gamma^2B_z^2-16J^2(1+\Gamma^2)m]^2m \tag{13}$$

for the square magnetization $m=\frac{1}{4}(\mathbf{S}_A+\mathbf{S}_B)^2$ (see Appendix A). Once m is known, $\mathbf{S}_A$ and $\mathbf{S}_B$ can be calculated. Due to the translational symmetry of Eq. (1), each solution of Eq. (13) is twofold degenerate:

$$\mathbf{S}_{2n}=\mathbf{S}_A,\quad \mathbf{S}_{2n+1}=\mathbf{S}_B,$$
$$\mathbf{S}_{2n}=\mathbf{S}_B,\quad \mathbf{S}_{2n+1}=\mathbf{S}_A. \tag{14}$$

In that sense there may be one or three nontrivial states. We now compute expressions for the saddle-node lines in question. If an extremum of the polynomial (13) considered as a function of m is zero, new fixed points are created in a saddle-node bifurcation. The resulting bifurcation lines SN are drawn in Figs. 1 and 2 in a parameter plane that is spanned by the driving field and static field. They meet in the points a,c_a,c_b and form the boundaries of a region in which three noncollinear states coexist. Outside this region there is only one noncollinear state. Inside, the states may be numbered in increasing order of the square magnetization m. In that sense, a saddle-node bifurcation of solutions 1 and 2 forms the bottom of the triangular structure, while its left and right sides correspond to saddle-node bifurcations of the fixed points 2 and 3.

Magnetic resonance techniques commonly use weak driving fields and materials with correspondingly weak dissipa-

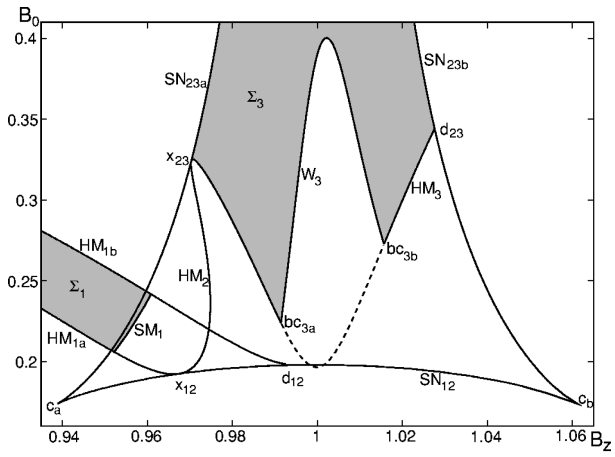

FIG. 2. Section of Fig. 1 with small driving fields near resonance containing the most interesting bifurcations. The saddle-node lines $SN_{12}, SN_{23a}, SN_{23b}$ bound a region with three nontrivial fixed points. They are labeled in the order of their magnetizations; the indices indicate which one is involved in the corresponding bifurcations. c_a and c_b are cusp points. In the shaded area Σ_1 a nontrivial stable stationary state exists. It is bounded by subcritical hard mode instabilities HM_{1a}, HM_{1b} and a subcritical soft mode line SM_1. This line becomes physically irrelevant after intersecting HM_{1a} and HM_{1b}. At the codimension-2 points x_{12} and x_{23}—on eigenvalue vanishes, two others are purely imaginary—the saddle-node and the hard mode touch each other. d_{12} and d_{23} represent Arnold-Takens-Bogdanov bifurcations. In the shaded area Σ_3, which is bounded by SN_{23a}, SN_{23b}, HM_3 and line W_3, solution 3 is stable. At W_3 there are imaginary eigenvalues for $k_c=\pi/2$. At the points $bc_{3a/b}$ solution 3 is critical for $k_c=0$ and for $k_c=\pi/2$. The broken part of line HM_3 does not correspond to a global maximum of an eigenvalue at $k_c=0$.

tion. Therefore, analytical results in this limit have a high relevance; we will first determine the corner points of this structure. For a cusp bifurcation, the unique solution of the polynomial is an inflection point. Consequently, the polynomial itself and its first and second derivative with respect to m must be zero. An expansion in terms of Γ in lowest order yields

$$B_0^4=\frac{1024}{27}J^2\omega^2\Gamma^2,$$
$$B_0^2=8(B_z-\omega)^2 \tag{15}$$

for the two cusp points c_a and c_b in Figs. 2 and 5. At

$$B_0^2=16J^2+\Gamma^2B_z^2,$$
$$\omega=(1+\Gamma^2)B_z \tag{16}$$

the polynomial and its first derivative vanishes at $m=1$. In this situation the spins of both sublattices become parallel. At this degenerate bifurcation point (point a in Fig. 1) the noncollinear states 2 and 3 bifurcate from the ferromagnetic state (see Sec. II and [3]).

At the saddle-node bifurcation the discriminant of third-order polynomial (13) vanishes; the polynomial has a single and a double root. Then for B_0 and $B_z-\omega\sim\Gamma^{1/2}$,

$$(B_z-\omega)^2[B_0^2+(B_z-\omega)^2]^3+4J^2\omega^2\Gamma^2[64J^2\omega^2\Gamma^2$$
$$+8(B_z-\omega)^4-20B_0^2(B_z-\omega)^2-B_0^4]=0 \tag{17}$$

holds. For $B_z-\omega\ll\Gamma^{1/2}$ (17) is solved by $B_0^4=64\Gamma^2\omega^2J^2$, which describes the saddle-node line SN_{12} at the bottom. The lateral saddle-node lines SN_{23} can be approximated by $B_0^2=4J^2\Gamma^2\omega^2/(B_z-\omega)^2+(B_z-\omega)^2$.

For a further study of the instabilities of the noncollinear states, it is useful to apply the stereographic projection in the direction of $\mathbf{S}_A+\mathbf{S}_B$ as outlined in Appendix A. It is possible to relate stationary states of $\mathbf{S}_{2n},\mathbf{S}_{2n+1}$ to real numbers $z_{2n}=x, z_{2n+1}=-x$ on the complex plane. The dynamics of the complex deviations Δz from equilibrium ($z_{2n}=x+\Delta z_{2n}, z_{2n+1}=-x+\Delta z_{2n+1}$) is governed by

$$\Delta\dot{z}_{2n}=+2(Q'+iQ'')x\Delta z_{2n}+(Q'+iQ'')\Delta z_{2n}^2-4J(i-\Gamma)\frac{1-x^2}{1+x^2}\Delta z_{2n}+J(i-\Gamma)\Bigg[(2x+\Delta z_{2n}-\Delta z_{2n+1})$$
$$\times\frac{1+(x+\Delta z_{2n})(-x+\Delta z_{2n+1}^*)}{1+(-x+\Delta z_{2n+1})(-x+\Delta z_{2n+1}^*)}+(2x+\Delta z_{2n}-\Delta z_{2n-1})\frac{1+(x+\Delta z_{2n})(-x+\Delta z_{2n-1}^*)}{1+(-x+\Delta z_{2n-1})(-x+\Delta z_{2n-1}^*)}-4x\frac{1-x^2}{1+x^2}\Bigg], \tag{18}$$

$$\Delta\dot{z}_{2n+1}=-2(Q'+iQ'')x\Delta z_{2n+1}+(Q'+iQ'')\Delta z_{2n+1}^2-4J(i-\Gamma)\frac{1-x^2}{1+x^2}\Delta z_{2n+1}-J(i-\Gamma)\Bigg[(2x-\Delta z_{2n+1}+\Delta z_{2n+2})$$
$$\times\frac{1+(-x+\Delta z_{2n+1})(x+\Delta z_{2n+2}^*)}{1+(x+\Delta z_{2n+2})(x+\Delta z_{2n+2}^*)}+(2x-\Delta z_{2n+1}+\Delta z_{2n})\frac{1+(-x+\Delta z_{2n+1})(x+\Delta z_{2n}^*)}{1+(x+\Delta z_{2n})(x+\Delta z_{2n}^*)}-4x\frac{1-x^2}{1+x^2}\Bigg]. \tag{19}$$

Q', Q'', x are functions of the external fields (see Appendix A for their definition). Due to the different orientation of the sublattices $\mathbf{S}_{2n}$ and $\mathbf{S}_{2n+1}$ in the stationary state the variables Re Δz, Im Δz at the lattice sites $2n$ and $2n+1$ are governed by different differential equations. Consequently, the system can be regarded as a chain of two different types of nonlinear two-dimensional oscillators. They may be combined in a four-dimensional vector field.

For the stability analysis we linearize the equations of motion (18),(19), insert the Bloch wave

$$\begin{pmatrix} \text{Re } \Delta z_{2n} \\ \text{Im } \Delta z_{2n} \\ \text{Re } \Delta z_{2n+1} \\ \text{Im } \Delta z_{2n+1} \end{pmatrix} = \begin{pmatrix} u_1 e^{ik2n} \\ u_2 e^{ik2n} \\ u_3 e^{ik(2n+1)} \\ u_4 e^{ik(2n+1)} \end{pmatrix} + \text{c.c.} \tag{20}$$

and obtain the Jacobian

$$2\begin{pmatrix} Q'x+J\Gamma & -Q''x+J & -J\Gamma q\cos k & J\cos k \\ Q''x-J & Q'x+J\Gamma & Jq\cos k & J\Gamma\cos k \\ -J\Gamma q\cos k & J\cos k & -Q'x+J\Gamma & Q''x+J \\ Jq\cos k & J\Gamma\cos k & -Q''x-J & -Q'x+J\Gamma \end{pmatrix} \tag{21}$$

with $q=8x^2/(1+x^2)^2-1$ and $-1\leqslant q\leqslant 1$. The wave vector k_c is restricted to the Brillouin zone $[-\pi/2,\pi/2]$. The coefficients of the characteristic polynomial

$$\lambda^4+K_3\lambda^3+K_2\lambda^2+K_1\lambda+K_0=0 \tag{22}$$

are given explicitly in Appendix B. Because of the nearest-neighbor coupling, the coefficients of Eq. (22) depend on the wave number k only via cos $2k$ and cos $4k$.

The condition $K_0=0$ for one vanishing eigenvalue at $k_c=0$ yields the saddle-node bifurcations that were described above. A zero eigenvalue at $k_c\neq 0$ indicates a soft-mode instability. Purely imaginary eigenvalues are obtained if $K_1^2-K_1K_2K_3+K_0K_3^2=0$ and $K_1/K_3>0$ hold. For $k_c=0$ and $k_c\neq 0$, the instability is designated as hard mode and wave instability, respectively (Fig. 3). All these bifurcation conditions have the form

$$d_0+d_2\cos 2k+d_4\cos 4k=0. \tag{23}$$

The characteristic polynomial can be studied analytically in part. It reveals an intricate bifurcation scenario. Here we give an overview of our results while we defer their derivation to Appendix B.

Within the shaded areas Σ_1 and Σ_3 in Fig. 2 there is one stable stationary state, while outside all states are unstable. Therefore, noncollinear states are stable for sufficiently strong driving fields. Σ_1 is bounded by the two hard-mode instabilities HM_{1a} and HM_{1b} and the soft-mode instability SM_1 (the index 1 refers to fixed point 1). The area Σ_3, in which fixed point 3 is stable, has the two saddle-node lines SN_{23a} and SN_{23b}, the hard-mode line HM_3 and the line W_3 as its boundaries. The last line represents a wave instability occurring at $k_c=\pi/2$ with $\omega\neq 0$. As cos $k_c=0$, it takes place for

$$Q'x=-J\Gamma. \tag{24}$$

Its critical eigenvectors

$$u_c/u_c^*=\frac{1}{\sqrt{2}}\begin{pmatrix} 1 \\ \pm i \\ 0 \\ 0 \end{pmatrix} \tag{25}$$

have the eigenvalues $\lambda=\pm i2(-Q''x+J)$. Consequently, neighboring spins on one sublattice are excited with opposite phases

$$\Delta\mathbf{S}_{2n+2}=\Delta\mathbf{S}_{2n}e^{2ik_c}=-\Delta\mathbf{S}_{2n} \tag{26}$$

while spins of the other sublattice remain unchanged. In analogy to the instability (11) at $k_c=\pi$, it describes a splitting of a sublattice into two new sublattices [Fig. 3(c)].

If the condition for imaginary eigenvalues is written in the form (23), HM_3 and W_3 correspond to $d_0+d_2+d_4=0$ and $d_0-d_2+d_4=0$, respectively. At the intersection points bc, there are two pairs of imaginary eigenvalues at $k_c=0$ and $k_c=\pi/2$. They correspond to $d_0+d_4=0$, $d_2=0$.

A particularly interesting bifurcation of codimension 3 is given if $d_0=d_2=d_4=0$. At this point (gc in Fig. 4) the real part of two eigenvalues vanishes for all k_c. This bifurcation will be studied in Sec. V.

It is worthwhile to determine the position of HM_3 and W_3 at exact resonance $B_z-\omega=0$. In Appendix B we find

$$B_0^2=16J^2\left(1-\frac{4J^2}{B_z^2}\right) \tag{27}$$

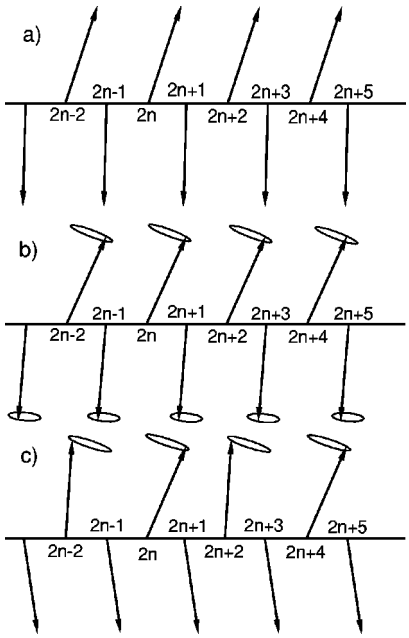

FIG. 3. Sketch of a noncolinear state (a), a hard mode instability (b), and of the instability W_3 (c): Neighboring spins $\mathbf{S}_{2n}$ and $\mathbf{S}_{2n+2}$ get opposite phases, $\mathbf{S}_{2n}$ and $\mathbf{S}_{2n+4}$ are again parallel. The sublattice with odd indices remains unchanged.

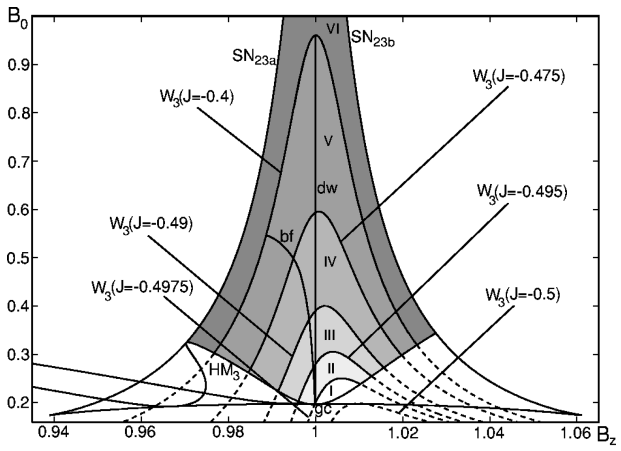

FIG. 4. Near $B_z^2-4J^2=0$ the wave instability W_3 invades the stability region S_3 rapidly. The lines W_3 are plotted for several coupling parameters $-0.5\leqslant J\leqslant -0.4$, SN and HM_3 only for $J=-0.49,\omega=1,\Gamma=0.01$. Where the lines are broken, the critical eigenvalue is not a global maximum of the spectrum. For $J=-0.4$, solution 3 is stable only in domain VI, for $J=-0.475$ it is stable in V and VI, etc. For $J=-0.5$ it is stable in I–VI and W_0 does not appear. bf and dw are codimension-2 lines in the B_0-B_z-J parameter space. On the right side of the degeneration point dw, the bifurcation W_3 is subcritical while on the left side of bf it is Benjamin-Feir unstable. dw and bf meet in the point gc $(J=-0.4975)$, which is critical for all wave numbers.

for the resonance point on W_3. This point is near to the maximum of this bifurcation line (see Figs. 4 and 5). The point of intersection of HM_3 and the resonance line is given by

$$B_0^4=64J^2\Gamma^2\omega^2 \tag{28}$$

and is near to the minimum value of the bifurcation line. These formulas reveal a resonance phenomenon between the internal exchange field J and the external static field B_z. While the saddle-node and hard-mode lines are quite insensitive to variations of J (they are plotted for $J=-0.49$ in Fig. 4), line W_3 is highly sensitive to variations of J near $4J^2=B_z^2$. Above this threshold W_3 invades the domain of existence of fixed point 3 strongly, thereby destabilizing it in a wide range (Fig. 4). In experimental situations where J is a material constant, the same can be achieved by varying B_z and ω.

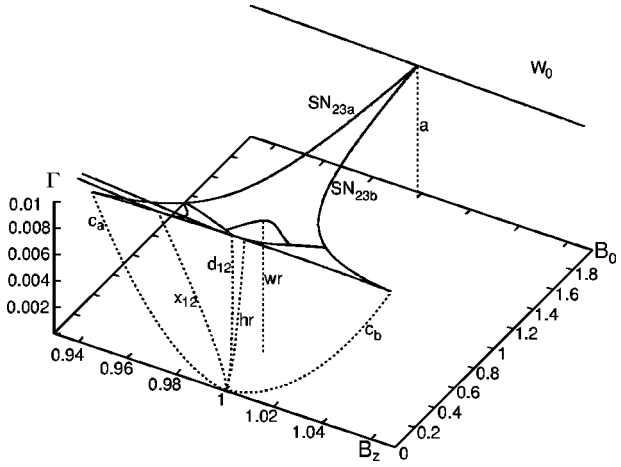

FIG. 5. Asymptotic behavior of codimension-2 bifurcations for weak damping. The solid lines in the B_0-B_z plane at $\Gamma=0.01$ are the bifurcation lines of Fig. 2. The dotted lines show the analytical expressions given in the text for the codimension-2 bifurcations c_a, c_b, a, x_{12}. d_{12} and the resonance points hr and wr of HM_3 and W_3 as functions of Γ,B_0,B_z.

Finally as is shown in Appendix B near resonance some interesting codimension two bifurcations occur:

Line HM_{1b} meets line SN_{12} in point d_{12}. This case is characterized by the linear part

$$\begin{pmatrix} 0 & 1 \\ 0 & 0 \end{pmatrix} \tag{29}$$

and represents an Arnold-Takens-Bogdanov bifurcation [19].

Line HM_{1a} meets line SN_{12} in point x_{12}. The corresponding linear part is

$$\begin{pmatrix} 0 & 0 & 0 \\ 0 & 0 & -\omega \\ 0 & \omega & 0 \end{pmatrix}. \tag{30}$$

Following the hard-mode line HM_2 of fixed point 2 (which is always unstable) one reaches the point x_{23}, which is again of the type (30). The points x_{23} on the saddle-node line SN_{23a} and d_{23} on the saddle-node line SN_{23b} are connected by the hard-mode line HM_3 of fixed point 3; d_{23} is again of the type (29).

For small values of Γ, d_{12} is located at (from $K_0=0,K_1=0$)

$$B_z(B_z-\omega)=-\frac{B_0^2}{8}, \tag{31}$$

$$64\Gamma^2\omega^2J^2=B_0^4, \tag{32}$$

while x_{12} is given by (from $K_0=0,K_1^2-K_1K_2K_3+K_0K_3^2=0$)

$$B_z(B_z-\omega)=-\frac{7}{8}B_0^2 \tag{33}$$

and again Eq. (32). These conditions are asymptotically exact for $\Gamma,B_0,B_z-\omega\to 0$ and they excellently agree with the numerical results for $\Gamma=0.01$ (Fig. 5).

In the context of pattern formation, the lines HM_{1a}, HM_{1b}, SM_1, HM_3, and W_3 are relevant because they concern stable solutions. The physical question is now whether these instabilities lead to stable short and long scale patterns.

V. AMPLITUDE EQUATIONS FOR THE WEAKLY NONLINEAR REGIME

The dynamics beyond the instabilities is governed by nonlinear terms. At threshold, a single mode is critical. It represents an ideal pattern. Slightly above threshold adjacent modes become unstable, also giving rise to slow spatial and temporal modulations

$$A(\tau_1,\ldots,\xi_1,\ldots)e^{i(k_cn+\omega t)}u_c+\text{c.c.} \tag{34}$$

u_c is the critical eigenvector [cf. Eq. (C14), Appendix C]. The dynamics of these structures is described by amplitude equations. A systematic general derivation for amplitude equations of oscillator chains is established in Appendix C. It reduces the dynamical behavior of the dissipative spin system to the Ginzburg-Landau equation

$$\dot{A} = \mu A + D\partial_x^2 A + rA^2 A^*. \tag{35}$$

The real part of the diffusion coefficient $D = -\frac{1}{2}\partial^2\lambda/\partial x^2$ is positive. For a negative real part of r, the equation saturates. Rescaling amplitude, phase, space, and time coordinates appropriately, one obtains

$$\dot{A} = \mu A + (1 + ic_1)\partial_x^2 A - (1 - ic_3)A^2 A^* \tag{36}$$

with $c_1 = \mathrm{Im}\,(D)/\mathrm{Re}\,(D)$ and $c_3 = -\mathrm{Im}\,(r)/\mathrm{Re}\,(r)$.

The amplitude equation contains two decisive pieces of information of the pattern formation beyond the instability: Firstly, it settles the stability of the short scale patterns linked to the critical eigenvector's wave number. Secondly, depending on its coefficients it categorizes the long scale patterns under the solutions of the complex Ginzburg-Landau equation [21]. Traveling waves as its most simple solutions should be observable as stripe patterns under magneto-optical observation.

Although neighboring spins have opposite phases at the instability (11), their amplitude is a smooth function of the space coordinate near threshold. The amplitude equation saturates; the coefficients are $c_1 = -1/\Gamma, c_3 = 1/\Gamma$. Because of $1 - c_1 c_3 = 1 + 1/\Gamma^2 > 0$, there is no Benjamin-Feir instability.

Any attempt to derive amplitude equation for the noncollinear case starting directly from Eq. (19) would be hopelessly complicated because of the algebraic structure of the four-dimensional field. In addition, spins on neighboring lattice sites, i.e., spins belonging to different sublattices, are influenced by different effective fields. Consequently, two different sorts of oscillators are arranged alternately on the chain. A general derivation for the cofficients of the amplitude equation is given in Appendix C. This formalism is transferred to chains of two different sorts of oscillators in Appendix D.

As a consequence of the inversion symmetry, $\lambda' = 0$ holds for bifurcations in the center and at the boundary of the Brillouin zone; for soft-mode bifurcations this is true anyway. Hence the drift velocity (C19) is zero. The diffusion coefficient follows by differentiating Eq. (22) twice

$$\lambda'' = -\frac{K_0'' + \lambda K_1'' + \lambda^2 K_2'' + \lambda^3 K_3''}{K_1 + 2\lambda K_2 + 3\lambda^2 K_3 + 4\lambda^3} \tag{37}$$

and inserting $\lambda = i\omega = \sqrt{-K_1/K_3}$.

The third order coefficient, which is responsible for saturation, is influenced by the quadratic and cubic terms of the original equation of motion. They are contained in the tensors $C_{i,j}^{\alpha,\beta}, D_{i,j,k}^{\alpha,\beta,\gamma}$ of Appendix C, which are needed in order to compute the coefficient c_3.

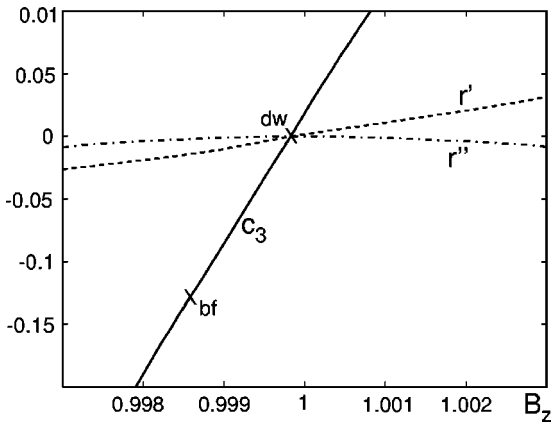

FIG. 6. The real and imaginary parts of the third order coefficient of W_3 for $J = -0.49$, r', r'', and $c_3 = -r''/r'$ vanish simultaneously.

In particular considering instability (24), which occurs at the margin of the Brillouin zone and concerns a system of two sublattices, its excitations may be written as [using Eq. (25)]

$$A(\epsilon 2n)\frac{1}{\sqrt{2}}\begin{pmatrix}1\\ i\end{pmatrix}e^{i(\pi/2)(2n)} + \text{c.c.}, \tag{38}$$

$$A(\epsilon(2n+1))\begin{pmatrix}0\\ 0\end{pmatrix}e^{i(\pi/2)(2n+1)} + \text{c.c.} \tag{39}$$

As a consequence, only the even numbered sublattice is involved. This splits into two new sublattices. Neighboring spins on this sublattice acquire opposite phases. The formation of more then two sublattices is a well-known experience in magnetostatics, e.g., in hidden antiferromagnetism. Interestingly, such a phenomenon is encountered here as a dynamical response to a homogeneously driving field.

The simplicity of the critical eigenvector (38), (38) makes the computation of the third order coefficient much easier: $\tilde{\Gamma}$ (C33) simplifies and Δ (C34) vanishes altogether. The remaining terms have been computed numerically.

The real and imaginary parts of the third order coefficient of W_3 are plotted in Fig. 6 for $J = -0.49$. The sign of the real part of the third order coefficient changes at $B_z \approx \omega$ (dw in Fig. 6; this codimension-2 bifurcation is plotted as a line with the parameter J in Fig. 4). In addition c_3 vanishes at dw. For $B_z < \omega$ the bifurcation W_3 is supercritical ($\mathrm{Re}\, r \equiv r' < 0$); the third order guarantees saturation so that the perturbation theory is valid. For $B_z > \omega$ it is subcritical and the dynamics leaves the vicinity of the stationary state.

Furthermore a Benjamin-Feir instability takes place at $c_1 c_3 = 1$ (bf has codimension 2 and is again plotted as a line in Fig. 4). Consequently stable plane wave solutions near W_3 are only possible between the lines bf and dw. Figure 4 shows that the Benjamin-Feir stable bifurcation W_3 is also obtained for small driving fields. In this domain, ideal and periodically modulated 3-sublattice solutions are stable, while in the Benjamin-Feir-unstable domain one expects phase turbulence as long scale pattern.

For $B_z > \omega$ the dynamics is not saturated by third order terms ($r' > 0$) and leaves the vicinity of the stationary solution.

Analogously, the amplitude equations arising in the context of the hard-mode instabilities HM_{1a}, HM_{1b}, HM_3, and the soft-mode instability SM_1 can be calculated. While the hard-mode instability HM_3 turns out to be supercritical which admits a description by a complex Ginzburg-Landau-equation, the instabilities HM_{1a} and HM_{1b} are subcritical. The soft-mode instability SM_1 corresponds to a real Ginzburg-Landau equation. As the sign of the third order coefficient is positive for SM_1, the bifurcation is subcritical and no pattern formation near the stationary state takes place.

To conclude, only instabilities at $k_c = 0$ and $k_c = \pi/2$ can lead to stable patterns. The magnetization of the stationary state is perpendicular to the external magnetic field. Variations arising from the instability contribute linearly to M_z.

VI. AMPLITUDE TURBULENCE NEAR A CODIMENSION-3 BIFURCATION

The Benjamin-Feir line and the degenerate-wave line meet tangentially at the codimension-3 bifurcation gc. At this point, the diffusion coefficient D is purely imaginary while the Hopf coefficient vanishes; one finds $c_1 \to -\infty$ and $c_3 \to 0$. The real part of the critical eigenvalues is identically zero for all k, while the imaginary part is nonzero. Therefore all k modes become critical simultaneously and one expects that waves of all length scales contribute to the spatiotemporal dynamics. Such disorder phenomena cannot be studied by amplitude equations, which require separate critical wave numbers. At gc a transition of W_3 from supercritical to subcritical is involved; for parameter values where the real part of an eigenvalue is k independent and positive, the dynamics leaves the vicinity of the stationary state.

The energy distribution over the k modes can be studied numerically in the supercritical region $B_0 \leqslant B_{0gc}$, $B_z \leqslant B_{zgc}$ where the system is saturated by third order terms. In this region the real part of the eigenvalue spectrum is very flat; it has its positive maximum at $k = 0$ and its negative minimum at $k = \pi/2$. The nonlinear terms depend on the wave number and provide a coupling mechanism of the modes. Correspondingly, the spatial power spectrum (Fig. 7) is maximal at $k = 0$ and exhibits broadband contributions for $|k| < \pi/5$. The excitation of the k modes in this area indicates turbulent spatiotemporal dynamics even in the short length scale of the lattice constant. A histogram of the magnetization shows a Gaussian distribution. The eigenvalue spectrum and the power spectrum suggest an interpretation similar to chemical turbulence of Kuramoto-Shivashinsky equation [24]: the energy is transported by nonlinear mode coupling from the long scales related to the homogeneous driving field to small scales where it is dissipated. But unlike this description of spatially slow phase variations, at the instability gc all length scales are involved. Such a globally critical bifurcation is known in two dimensions where a simultaneous instability on the circle $|\mathbf{k}| = k_c$ produce spatially turbulent structures if the modes are coupled appropriately [25].

As a result of the simple k dependance of the next neighbor coupling containing only terms $\sim 1, \cos 2k, \cos 4k$, Eq. (23), only three conditions are required for this bifurcation.

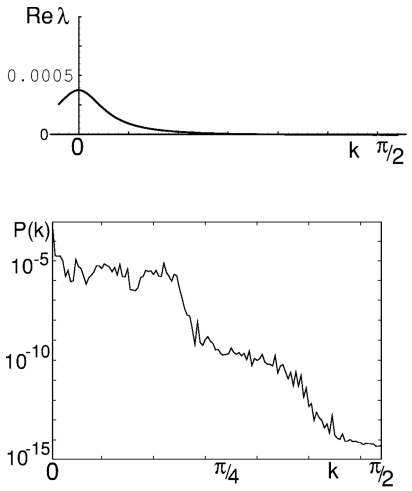

FIG. 7. Eigenvalue spectrum and power spectrum at $B_0 = 0.19798, B_z = 0.99945$ near point gc. While at gc the critical eigenvalue has a zero real part for all wave numbers, for slightly smaller values of B_0 and B_z the eigenvalue spectrum has a flat maximum at $k = 0$ and is negative for $k = \pi/2$. The power spectrum reveals broadband contributions in the center of the Brillouin zone (roughly for $|k| < \pi/5$) while to its boundary $k = \pi/2$ it slopes down. It has been computed by numerical integration of a set of 512 spins with periodic boundary conditions.

The parameter values of this bifurcation can be easily computed: at gc HM_3, W_3 and $B_z - \omega = 0$ intersect. The corresponding value of J can be computed by equating (27) and (28). One finds

$$B_z^2 - 4J^2 = \Gamma B_z^2 \tag{40}$$

and thus $J = -B_z(1 - \Gamma/2)/2 = -0.4975$, which agrees with the numerical value (Fig. 4). This shows that the external field must offset the exchange interaction, requiring the latter to be relatively weak.

VII. CONCLUSIONS

We have studied nonequilibrium pattern formation of a driven dissipative one dimensional antiferromagnet that exhibits instabilities with wavelengths of the order of the lattice constant. Classical continuum models of antiferromagnets are based on the assumption that both sublattices are smooth over such distances. But in the case of short wavelength instabilities this supposition breaks down. This necessitates a fully discrete description of the system.

The noncollinear orientation of the sublattice magnetizations in the stationary state showing these instabilities is a common phenomenon in magnetism. In our system it is caused by the driving field balanced by a Landau-Lifshitz damping. The resulting magnetization of the stationary states is perpendicular to the static magnetic field, whereas instabilities of this state lead to a magnetization parallel to the z axis, effecting a Faraday rotation of light. Similar effects are likely in weak ferromagnets, where canting of equilibrium states is induced by anisotropic superexchange or a single ion anisotropy with alternating preferred axes.

We have detected a variety of instabilities by investigating the possible local codimension-one and -two bifurcations

systematically. Short wavelength instabilities are encountered for relatively weak driving fields $B_0 \sim J^{1/2}\Gamma^{1/2}$ near resonance. It is a generic result that there are instabilities in the center and at the boundary of the Brillouin zone. The latter bifurcations describe a coupling of the spatially homogeneous driving field to short wavelength excitations (optical spin waves). They occur when the static external field offsets the exchange field.

To determine the physical status of spatial patterns above these instability thresholds, a weakly nonlinear analysis has been performed. A general scheme allowing the treatment of one- and two-oscillator chains has been derived. Avoiding any unsystematic assumptions, a continuous amplitude equation for the bifurcating solutions emerges. It provides explicit formulas for a complex Ginzburg-Landau equation that governs slow variations of an ideal solution. Its application to our system shows that stable long scale patterns are formed on short scale structures related to lattice splitting. Saturation is also verified at a hard mode instability. The instabilities far from resonance are subcritical; therefore, they do not lead to stable nonequilibrium patterns.

An abrupt order/disorder transition results from a codimension-3 bifurcation in which a Benjamin-Feir line and a degenerated wave instability line meet. All wave numbers are critical at this instability; numerical findings indicate a direct transition to turbulentlike dynamics. The relatively low codimension of this bifurcation is again a generic result in the case of nearest neighbor coupling.

While the bifurcation scenario itself shows no qualitative changes for weak damping and weak driving fields, the decreasing diffusion constant restricts the validity of amplitude equations to long time and length scales. For that, films with relatively high linewidths seem to be good candidates for the observation of patterns. Anisotropic, quasi-one-dimensional materials might serve as the most simple prototypes for magnetooptic observations of stripe structures.

ACKNOWLEDGMENTS

Valuable discussions with Dr. H. Benner and Dr. W. Just are gratefully acknowledged. This work was performed within a program of Sonderforschungsbereich 185, Darmstadt, Frankfurt.

APPENDIX A

Stereographic projection

The class of solutions of Eq. (1) pertaining to two homogeneous sublattices can be described in terms of two interacting spin oscillators $\mathbf{S}_A \equiv \mathbf{S}_{2n}, \mathbf{S}_B \equiv \mathbf{S}_{2n+1}$. To determine their stationary states (13) and their stability properties we make use of the conservation of modulus of $|\mathbf{S}_{A/B}|=1$ by projecting the equation of motion

$$-\dot{\mathbf{S}}_A = \mathbf{S}_A \times (\mathbf{B} - \boldsymbol{\omega} + 2J\mathbf{S}_B) + \Gamma \mathbf{S}_A \times [\mathbf{S}_A \times (\mathbf{B} + 2J\mathbf{S}_B)] \tag{A1}$$

along some arbitrary direction $\mathbf{e}_\zeta = \mathbf{e}_\xi \times \mathbf{e}_\eta$ into the $\mathbf{e}_\xi$-$\mathbf{e}_\eta$ plane where $\mathbf{e}_\xi$ and $\mathbf{e}_\eta$ are identified with the real and imaginary axes of the complex number plane, respectively (Fig. 8). This yields

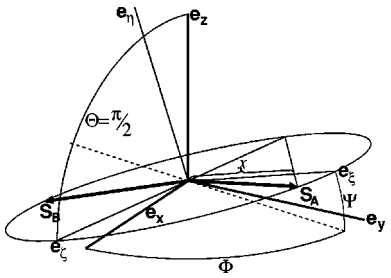

FIG. 8. A coordinate system $\mathbf{e}_\xi, \mathbf{e}_\eta, \mathbf{e}_\zeta$ can be chosen in a way that a stereographic projection of $\mathbf{S}_{A/B}$ into the complex $\mathbf{e}_\xi$-$\mathbf{e}_\eta$ plane ($\mathbf{e}_\xi$ is the real axis, $\mathbf{e}_\eta$ is the imaginary axis) yields real numbers $\pm x$ for the stationary state. In this case $\mathbf{S}_{A/B}$ are symmetrical to the $\mathbf{e}_\zeta$ axis.

$$\begin{aligned}\dot{z}_A = {} & (i-\Gamma)B_\xi \frac{z_A^2-1}{2} - i(i-\Gamma)B_\eta \frac{1+z_A^2}{2} + (i-\Gamma)B_\zeta z_A \\ & - i\omega_\xi \frac{z_A^2-1}{2} - \omega_\eta \frac{1+z_A^2}{2} - i\omega_\zeta z_A + 2J(i-\Gamma) \\ & \times (z_A - z_B)\frac{1+z_A z_B^*}{1+z_B z_B^*},\end{aligned} \tag{A2}$$

where $z=(S_\xi + iS_\eta)/(1+S_\zeta)$; B_ξ, B_η, B_ζ and $\omega_\xi, \omega_\eta, \omega_\zeta$ are defined as the components of $\mathbf{B}=B_0\mathbf{e}_x + B_z\mathbf{e}_z$ and $\boldsymbol{\omega}=\omega\mathbf{e}_z$ in the directions $\mathbf{e}_\xi, \mathbf{e}_\eta$, and $\mathbf{e}_\zeta$, respectively. A corresponding equation holds for z_B. Projecting in the direction of the total magnetization $\mathbf{e}_\zeta \sim \mathbf{S}_A + \mathbf{S}_B$, one recognizes that the corresponding complex variables become located symmetrically with respect to the origin of the complex $\mathbf{e}_\xi$-$\mathbf{e}_\eta$-plane, i.e., $z_A = -z_B$. Finally $\mathbf{e}_\xi, \mathbf{e}_\eta$ can be determined so that $z_A = x, z_B = -x$ are real numbers on the $\mathbf{e}_\xi$ axis. This reduces the form of the fixed-point equations ($\dot{\mathbf{S}}_A = \dot{\mathbf{S}}_B = 0$) to

$$0 = Qx^2 \pm Rx + S \pm 4xJ(i-\Gamma)\frac{1-x^2}{1+x^2}. \tag{A3}$$

By comparison with Eq. (A2), the complex quantities Q, R, S are given as

$$Q = \frac{(i-\Gamma)B_\xi}{2} - \frac{i(i-\Gamma)B_\eta}{2} - \frac{i\omega_\xi}{2} - \frac{\omega_\eta}{2}, \tag{A4}$$

$$R = (i-\Gamma)B_\zeta - i\omega_\zeta, \tag{A5}$$

$$S = -\frac{(i-\Gamma)B_\xi}{2} - \frac{i(i-\Gamma)B_\eta}{2} + \frac{i\omega_\xi}{2} - \frac{\omega_\eta}{2}. \tag{A6}$$

Adding and subtracting the two equations (A3) and dropping the trivial solution $x=0$ leads to

$$0 = Qx^2 + S, \tag{A7}$$

$$0 = R + 4J(i-\Gamma)\frac{1-x^2}{1+x^2}. \tag{A8}$$

Obviously (A5) and (A8) force ω_ζ to be zero, i.e., $\mathbf{e}_\zeta$ must be perpendicular to $\boldsymbol{\omega}=\omega\mathbf{e}_z$. Introducing the Eulerian angles Φ,Θ, and Ψ which connect the two coordinate systems, we have $\Theta=\pi/2$ and consequently

$$B_\xi = B_0\cos\Psi\,\cos\Phi + B_z\sin\Psi,$$

$$B_\eta = -B_0\sin\Psi\,\cos\Phi + B_z\cos\Psi,$$

$$B_\zeta = B_0\sin\Phi. \tag{A9}$$

The quantities $Q=Q'+iQ''$, $S=S'+iS''$ and R may be written as

$$Q' = \frac{1}{2}(B_\eta-\omega_\eta-\Gamma B_\xi) = -\frac{\Gamma}{1+x^2}B_\xi$$

$$= -\frac{\Gamma}{1+x^2}(B_0\cos\Psi\,\cos\Phi + B_z\sin\Psi),$$

$$Q'' = \frac{1}{2}(B_\xi-\omega_\xi+\Gamma B_\eta) = \frac{1}{1+x^2}(B_\xi-\omega_\xi)$$

$$= \frac{1}{1+x^2}[B_0\cos\Psi\,\cos\Phi + (B_z-\omega)\sin\Psi],$$

$$S' = \frac{1}{2}(B_\eta-\omega_\eta+\Gamma B_\xi),$$

$$S'' = -\frac{1}{2}(B_\xi-\omega_\xi-\Gamma B_\eta),$$

$$R = (i-\Gamma)B_\zeta. \tag{A10}$$

Equations (A7) and (A8) lead to three real equations

$$B_\eta-\omega_\eta = -\Gamma B_\xi\frac{1-x^2}{1+x^2}, \tag{A11}$$

$$(B_\xi-\omega_\xi)\frac{1-x^2}{1+x^2} = \Gamma B_\eta, \tag{A12}$$

$$B_\zeta = -4J\frac{1-x^2}{1+x^2}. \tag{A13}$$

Then inserting the definitions (A9) in Eqs. (A11), (A12), (A13), we find for the three unknowns Φ,Ψ, and x,

$$\left(-B_0\cos\Phi+\Gamma B_z\frac{1-x^2}{1+x^2}\right)\sin\Psi+\left((B_z-\omega)+\Gamma B_0\cos\Phi\frac{1-x^2}{1+x^2}\right)\cos\Psi=0, \tag{A14}$$

$$\left(-\Gamma B_0\cos\Phi-(B_z-\omega)\frac{1-x^2}{1+x^2}\right)\sin\Psi+\left(\Gamma B_z-B_0\cos\Phi\frac{1-x^2}{1+x^2}\right)\cos\Psi=0 \tag{A15}$$

$$\cos^2\Phi = 1-\frac{16J^2m}{B_0^2}. \tag{A16}$$

Eliminating Ψ and Φ, we end up with the third order polynomial (13) of the square magnetization $m=[(1-x^2)/(1+x^2)]^2=\frac{1}{4}(\mathbf{S}_A+\mathbf{S}_B)^2$; it depends only on the physical parameters B_0,B_z,ω,J,Γ. It is often more convenient to use the quantities Q',Q'',x,J,Γ as independent parameters instead of B_0,B_z,ω,J,Γ. This allows us to compute bifurcations without solving Eq. (13). The physical quantities B_0,B_z,ω can be expressed through these new parameters: using (A7) to express S in terms of Q, one may solve the four equations (A10) for $B_\xi,B_\eta,\omega_\xi,\omega_\eta$ in terms of Q',Q'' and x as well. Noting that Eq. (A8) implies Eq. (A13) and $\omega_\zeta=0$ we get

$$B_\xi = -\frac{Q'}{\Gamma}(1+x^2)\omega_\xi = -\left(\frac{Q'}{\Gamma}+Q''\right)(1+x^2),$$

$$B_\eta = \frac{Q''}{\Gamma}(1-x^2)\omega_\eta = \left(\frac{Q''}{\Gamma}-Q'\right)(1-x^2),$$

$$B_\zeta = -4J\frac{1-x^2}{1+x^2}\omega_\zeta = 0. \tag{A17}$$

Since $\omega=\sqrt{\omega_\xi^2+\omega_\eta^2+\omega_\zeta^2}$, $B_z\omega=B_\xi\omega_\xi+B_\eta\omega_\eta$, and $B_0=\sqrt{(\mathbf{B}_0+\mathbf{B}_z)^2-B_z^2}$, we have three relations that can be interpreted as effecting a transition from the original parameters B_0,B_z,ω to a new set of parameters Q',Q'',x leaving J and Γ fixed, and vice versa.

APPENDIX B

Analytical calculation of bifurcations for weak damping

All local bifurcations are determined by the roots of the characteristic polynomial (22) $\lambda^4+K_3\lambda^3+K_2\lambda^2+K_1\lambda+K_0=0$ with

$$K_0=16\{(1-\cos^2k)J^4(1+\Gamma^2)(1-q^2\cos^2k)$$
$$+x^2J^2\cos^2k[Q''^2(1+q^2)-2Q'Q''\Gamma(1-q)^2$$
$$+2Q''^2\Gamma^2q+Q'^2(\Gamma^2+2q+\Gamma^2q^2)]$$
$$+x^2J^2[2(Q'+Q''\Gamma)^2-2(Q''-Q'\Gamma)^2]$$
$$+x^4(Q'^2+Q''^2)^2\}, \tag{B1}$$

$$K_1=8\{(1+\Gamma^2)\Gamma J^3 2[(1+q^2)\cos^2k-2]$$
$$+4Jx^2[(Q'^2-Q''^2)\Gamma-2Q'Q'']\}, \tag{B2}$$

$$K_2=4\{J^2[2+6\Gamma^2-\cos^2k(\Gamma^2+2q+\Gamma^2q^2)]$$
$$-2x^2(Q'^2-Q''^2)\}, \tag{B3}$$

$$K_3=-8\Gamma J. \tag{B4}$$

If $K_0=K_1=0$, two eigenvalues vanish simultaneously, while for $K_0=K_1(K_1-K_2K_3)+K_0K_3^2=0, K_1K_3>0$ one has one zero and two imaginary eigenvalues. From these formulas one can obtain analytical expressions for local codimension-two bifurcations at $k_c=0$ in the limit of small damping. We assume scaling laws for the driving field $B_0\sim\Gamma^\beta$, the detuning $B_z-\omega\sim\Gamma^\rho$, and the magnetization $m\sim\Gamma^\mu$. β, ρ, μ are positive real numbers to be determined in the course of the subsequent calculations. As the left-hand side of Eq. (22) must be positive, one has to require $\mu\geqslant 2\beta$. By equating the left- and right-hand sides of Eq. (22), one gets $2+2\beta=\min(4\beta,4\rho,4,2\mu)+\mu$ or equivalently $1\geqslant\min(2\beta,2\rho)$. We restrict ourselves to vanishing wave numbers $k_c=0$. The leading terms of the condition $K_0=0$ are always contained in

$$Q''^2(Q''^2-4J^2m)+4J^2Q'^2=0 \tag{B5}$$

while $K_1=0$ yields

$$2Q'Q''+2J^2\Gamma m+Q''^2\Gamma=0. \tag{B6}$$

For $\beta=\frac{1}{2},\rho=1$, all terms of Eq. (B6) are of order 2, while Eq. (B5) is reduced to $Q''^2-4J^2m=0$. The polynomial (13) is simply $\Gamma^2\omega^2=(B_0^2-16J^2m)m$. From Eqs. (B5) and (A16) it follows that $B_0^2=32J^2m, \cos^2\Phi=\frac{1}{2}, \cos\Psi=1$. We get $\sin\Psi=(B_z-\omega)/(B_0\cos\Phi)=\sqrt{2}(B_z-\omega)/B_0$ and finally equations (31), (32), that is, point d_{12} in Fig. 2.

Analogously, the condition $K_1(K_1-K_2K_3)+K_0K_3^2=0$ for two imaginary eigenvalues is reduced to

$$Q'^2Q''^2-2J^2\Gamma^2Q''^2m-J^4\Gamma^2m^2=0. \tag{B7}$$

Again Eqs. (B5) and (B7) can be fulfilled simultaneously only for $\beta=\frac{1}{2},\rho=1$ and together with $K_0=0$ this leads to Eqs. (32) and (33), which define point x_{12} in Fig. 2.

We now compute the intersection point of the bifurcation W_3 and the resonance line $B_z=\omega$. From Eqs. (A14) and (A15) we find for $B_z-\omega=0$

$$\Gamma B_z\frac{1-x^2}{1+x^2}=B_0\cos\Phi \tag{B8}$$

and

$$-\Gamma\frac{1-x^2}{1+x^2}\sin\Psi+\left[1-\left(\frac{1-x^2}{1+x^2}\right)^2\right]\cos\Psi=0 \tag{B9}$$

and consequently $\sin\Psi\approx 1$. As condition (13) that the solution be stationary reduces to $B_0^2-16J^2m=0$ for $B_z=\omega$, we obtain Eq. (27) by using $Q'=-(\Gamma B_\xi)/(1+x^2)=-(\Gamma B_z)/2$ and the bifurcation condition (24).

Similarly one can evaluate the resonance point $B_z=\omega$ of bifurcation HM_3. The leading terms of the condition $K_1(K_1-K_2K_3)+K_0K_3^2=0$ for two imaginary eigenvalues are

$$Q'^2-J^2m^2=0. \tag{B10}$$

Again inserting $Q'=-\Gamma B_z/2$ and $m=B_0^2/(16J^2)$ we get Eq. (28).

APPENDIX C

Amplitude equations for general oscillator chains

Multiple scale techniques for deriving amplitude equations have proved to be a powerful tool for the study of pattern formation [20] in hydrodynamics, liquid crystals, reaction-diffusion systems and magnetism [6,7] in the weakly nonlinear regime beyond an instability threshold.

In this section we adapt the theoretical framework for continuous systems [6,26–28] to general spatially discrete systems. Our derivation is performed in analogy to a recent discussion of partial differential equations [28]. In our concept, each member of an oscillator chain is described by the product of the eigenvector of a critical mode, a phase factor depending on the lattice site and an amplitude that varies slowly in space and time. The phase factor allows for short wavelength excitations where neighboring oscillators move out of phase. The slow variations of this ideal solution will be governed by a partial differential equation for the amplitude, which becomes smooth in the large aspect ratio. The coefficients of this equation determine the dynamics above threshold. We derive general expressions for these coefficients.

We treat a chain

$$\underline{\Phi}=[\phi(1)\cdots\phi(n),\phi(n+1),\cdots,\phi(N)]$$

of N oscillators $\phi(n)=\underline{\Phi}_{(n)}$ each of which has M degrees of freedom. The dynamics of this NM-dimensional system is described by

$$\dot{\underline{\Phi}}=\underline{\underline{\mathcal{L}}}\,\underline{\Phi}+\underline{\mathcal{N}}(\underline{\Phi}), \tag{C1}$$

where

$$\underline{\underline{\mathcal{L}}}=\underline{\underline{\mathcal{L}}}^{(0)}+\epsilon^2\underline{\underline{\mathcal{L}}}^{(2)}+\cdots \tag{C2}$$

is a matrix. $\underline{\underline{\mathcal{L}}}^{(0)}$ controls the instability, i.e., it leads to a marginally stable mode and ϵ^2 measures the distance to threshold. $\underline{\mathcal{N}}$ comprises all nonlinearities. We split $\underline{\underline{\mathcal{L}}}^{(0)}$ in $M\times M$ block matrices L_i and its eigenvectors $\underline{\underline{\Phi}}^{(\nu)}(k)$ in M-dimensional subvectors $\underline{\Phi}_{(n)}^{(\nu)}(k)=\phi^{(\nu)}(n,k)=e^{ikn}u^{(\nu)}(k)$:

$$\underline{\underline{\mathcal{L}}}^{(0)}\underline{\Phi}^{(\nu)}(k)=\begin{pmatrix} & & & \cdots & & & & 0 & 0 & 0 \\ 0 & \cdots & L_{-2} & L_{-1} & L_0 & L_1 & L_2 & \cdots & 0 & 0 \\ 0 & 0 & \cdots & L_{-2} & L_{-1} & L_0 & L_1 & L_2 & \cdots & 0 \\ 0 & 0 & 0 & \cdots & L_{-2} & L_{-1} & L_0 & L_1 & L_2 & \cdots \\ 0 & 0 & 0 & 0 & & & \cdots & & & \end{pmatrix}\begin{pmatrix} \cdot\cdot \\ e^{ik(n-1)}u^{(\nu)}(k) \\ e^{ikn}u^{(\nu)}(k) \\ e^{ik(n+1)}u^{(\nu)}(k) \\ \cdot\cdot \end{pmatrix}, \tag{C3}$$

where $L_\alpha, \alpha \neq 0$ is the linear part of the coupling to the αth neighbor while L_0 describes the linear dynamics of the oscillators ϕ. Introducing $L(k)=\Sigma_\alpha L_\alpha e^{ik\alpha}$ the eigenvalue equation

$$\underline{\underline{\mathcal{L}}}^{(0)}\underline{\Phi}^{(\nu)}(k)=\lambda^{(\nu)}(k)\underline{\Phi}^{(\nu)}(k) \tag{C4}$$

can be written as

$$L(k)u^{(\nu)}(k)=\lambda^{(\nu)}(k)u^{(\nu)}(k), \tag{C5}$$

where (ν) numerates the eigenvalues and vectors. The nonlinearity is given as a series of its mth powers:

$$\underline{\mathcal{N}}[\underline{\Phi}]=\sum_m \underline{\mathcal{N}}_m[\underline{\Phi}]. \tag{C6}$$

Of course the nonlinearities depend on the system parameters too and may therefore be expanded as $\underline{\mathcal{N}}_m=\underline{\mathcal{N}}_m^{(0)}+\epsilon^2\underline{\mathcal{N}}_m^{(2)}+\cdots$. As the second term contributes to the fourth order only, in the following only the first term will play a role. The most general quadratic term $(m=2)$ may be written as

$$(\underline{\mathcal{N}}_2[\underline{\Phi}])_{(n)}=\sum_{\alpha,\beta} C^{\alpha\beta}(\phi(n+\alpha),\phi(n+\beta)), \tag{C7}$$

where the j component of the real vector $C^{\alpha\beta}$ is defined explicitly as

$$C_{(j)}^{\alpha\beta}(\phi(n+\alpha),\phi(n+\beta))=\sum_{l,m} c_{jlm}^{\alpha\beta}\phi_l(n+\alpha)\phi_m(n+\beta). \tag{C8}$$

These components satisfy the symmetry relation

$$C^{\alpha\beta}(u,v)=C^{\beta\alpha}(v,u). \tag{C9}$$

Similarly, cubic terms may be decomposed as

$$\underline{\mathcal{N}}_3[\underline{\Phi}]_{(n)}=\sum_{\alpha,\beta,\gamma} D^{\alpha\beta\gamma}(\phi(n+\alpha),\phi(n+\beta),\phi(n+\gamma)), \tag{C10}$$

$$D_{(j)}^{\alpha\beta\gamma}(\phi(n+\alpha),\phi(n+\beta)\phi(n+\gamma))=\sum_{h,l,m} d_{jhlm}^{\alpha\beta\gamma}\phi_h(n+\alpha)\phi_l(n+\beta),\phi_m(n+\gamma). \tag{C11}$$

A scalar product may be defined via

$$\langle\underline{\Psi}|\underline{\Phi}\rangle=\frac{1}{N}\sum_n [\psi(n)|\phi(n)] \tag{C12}$$

Near an instability with the critical eigenvalues $\lambda^{(\nu_c)}(k=k_c)=-\lambda^{(\nu_c)}(-k_c)=i\omega_c$ and eigenvectors $u_c:=u^{(\nu_c)}(k_c)$ and $u_c^*:=u^{(\nu_c)}(-k_c)$, a perturbation scheme is set up by expanding the solution $\underline{\Phi}$ or ϕ of Eq. (C1) in terms of ϵ:

$$\phi(n)=\epsilon\phi(n)^{(1)}+\epsilon^2\phi(n)^{(2)}+\epsilon^3\phi(n)^{(3)}+\cdots. \tag{C13}$$

We require that the equations of motion that result by inserting this ansatz are fulfilled in each order of ϵ separately. In order to avoid secular terms, the right-hand sides of the equations arising in consecutive orders must be orthogonal to the critical left eigenvector. The resulting solvability conditions govern the dynamics of the amplitude A of the modulated state. It is introduced explicitly by

$$\phi(n)^{(1)}=u_c e^{i(k_c n+\omega_c t)}A(\tau_1,\tau_2,\ldots,\xi_1,\xi_2,\ldots)+\text{c.c.} \tag{C14}$$

and depends on the scaled coordinates

$$\tau_\mu=\epsilon^\mu t, \xi_\mu=\epsilon^\mu n \tag{C15}$$

with $\mu=0,1,2,\ldots$. In first order the equation of motion is the eigenvalue equation of the critical mode.

In second order the dynamics is governed by

$$\left(\frac{\partial}{\partial t}-\underline{\underline{\mathcal{L}}}^{(0)}\right)\underline{\Phi}^{(2)}=-\left[\left(\frac{\partial}{\partial\tau_1}-\underline{\underline{\mathcal{L}}}^{(0)}\right)\underline{\Phi}^{(1)}\right]^{(1)}+(\underline{\mathcal{N}}_2[\underline{\Phi}])^{(2)}. \tag{C16}$$

Considering the fact that $\phi^{(1)}(n)$ depends on ϵ via the arguments of the amplitude A, application of $\underline{\underline{\mathcal{L}}}^0$—compare Eq. (C3)—leads in first order to

$$\begin{aligned}(\underline{\underline{\mathcal{L}}}^0\underline{\Phi}^{(1)})_{(n)}^{(1)} &= \sum_\alpha L_\alpha u_c e^{ik_c\alpha}\left(A+\epsilon\alpha\frac{\partial A}{\partial\xi_1}+\cdots\right)^{(1)}e^{i(k_c n+\omega_c t)}+\text{c.c.} \\ &= -iL'(k_c)u_c e^{i(k_c n+\omega_c t)}\frac{\partial A}{\partial\xi_1}+\text{c.c.}\end{aligned} \tag{C17}$$

Multiplying Eq. (C16) with the critical left eigenvector $(\ldots,v_c e^{i(k_c n+\omega_c t)},\ldots)$, the following solvability condition emerges:

$$-i[v_c|L'(k_c)|u_c]\frac{\partial A}{\partial\xi_1}-(v_c|u_c)\frac{\partial A}{\partial\tau_1}=0. \tag{C18}$$

Note that $\mathcal{N}_2[\Phi]$ is orthogonal to the left eigenvector. As the real part of the critical eigenvalue has a maximum at k_c, with the drift velocity

$$V=\left.\frac{d\omega(k)}{dk}\right|_{k_c} \tag{C19}$$

it follows that

$$\frac{\partial A}{\partial \tau_1}=V\frac{\partial A}{\partial \xi_1}. \tag{C20}$$

With the abbreviation

$$\Gamma_a=\frac{1}{L(0)}\sum_{\alpha,\beta} e^{ik_c(\alpha-\beta)}C^{(\alpha\beta)}\{u_c,u_c^*\}, \tag{C21}$$

$$\Gamma_b=\frac{1}{L(2k_c)-2i\omega_c 1}\sum_{\alpha,\beta} e^{ik_c(\alpha+\beta)}C^{(\alpha\beta)}\{u_c,u_c\} \tag{C22}$$

and the inversion formula

$$\left(\frac{1}{L(k)}\right)_{\langle\nu_c\rangle}:=\sum_{\mu\neq\nu_c}\frac{1}{\lambda^{(\mu)}(k)}\frac{|u_k^\mu)(v_k^\mu|}{(u_k^\mu|v_k^\mu)}, \tag{C23}$$

the second order equation can be formally integrated:

$$\underline{\Phi}_{(n)}^{(2)}=-2\Gamma_a|A|^2-\Gamma_b e^{2i(k_cn+\omega_ct)}A^2-\Gamma_b^* e^{-2i(k_cn+\omega_ct)}\times(A^*)^2+\left(\frac{1}{L(k_c)-i\omega_c 1}\right)_{\langle\nu_c\rangle}(iL'(k_c)+V1)u_c e^{i(k_cn+\omega_ct)}\frac{\partial A}{\partial\xi_1}+\left(\frac{1}{L(-k_c)+i\omega_c 1}\right)_{\langle\nu_c\rangle}\times(iL'(-k_c)+V1)u_c^* e^{-i(k_cn+\omega_ct)}\frac{\partial A^*}{\partial\xi_1}+\cdots, \tag{C24}$$

where we have omitted transient terms and terms of the form of the first order solution (C14).

In the third order the equation of motion is

$$\left(\frac{\partial}{\partial t}-\underline{\underline{\mathcal{L}}}^{(0)}\right)\underline{\Phi}^{(3)}=-\left[\left(\frac{\partial}{\partial t}-\underline{\underline{\mathcal{L}}}^{(0)}\right)\underline{\Phi}^{(2)}\right]^{(1)}-\left[\left(\frac{\partial}{\partial t}-\underline{\underline{\mathcal{L}}}^{(0)}\right)\underline{\Phi}^{(1)}\right]^{(2)}+\underline{\underline{\mathcal{L}}}^{(2)}\underline{\Phi}^{(1)}+(\underline{\mathcal{N}}_2[\underline{\Phi}])^{(3)}+(\underline{\mathcal{N}}_3[\underline{\Phi}])^{(3)} \tag{C25}$$

with the linear inhomogeneities

$$\left[\left(\frac{\partial}{\partial t}-\underline{\underline{\mathcal{L}}}^{(0)}\underline{\Phi}^{(2)}\right)\right]_{(n)}^{(1)}=i[iL'(k_c)+V1]\left(\frac{1}{L'(k_c)-i\omega_c 1}\right)_{\langle\nu_c\rangle}(iL'(k_c)+V1)u_c e^{i(k_cn+\omega_ct)}\frac{\partial^2 A}{\partial\xi_1^2}+\text{c.c.}+\cdots, \tag{C26}$$

$$\left[\left(\frac{\partial}{\partial t}-\underline{\underline{\mathcal{L}}}^{(0)}\right)\underline{\Phi}^{(1)}\right]_{(n)}^{(2)}=u_c e^{i(k_cn+\omega_ct)}\frac{\partial A}{\partial\tau_2}-iL'(k_c)u_c e^{i(k_cn+\omega_ct)}\frac{\partial A}{\partial\xi_2}+\frac{(-i)^2}{2}L''(k_c)u_c e^{i(k_cn+\omega_ct)}\frac{\partial^2 A}{\partial\xi_2^2}+\text{c.c.}, \tag{C27}$$

where we have skipped nonresonant waves which are not proportional to $e^{i(k_cn+\omega_ct)}$. The contribution from quadratic terms is

$$(\underline{\mathcal{N}}_2[\underline{\Phi}])_{(n)}^{(3)}=\sum_{\alpha\beta} C^{(\alpha\beta)}\{\phi^{(1)}(n+\alpha),\phi^{(2)}(n+\beta)\}+\sum_{\alpha\beta} C^{(\alpha\beta)}\{\phi^{(2)}(n+\alpha),\phi^{(1)}(n+\beta)\} \tag{C28}$$

while the contribution from cubic terms is given by Eq. (C10). Multiplying Eq. (C25) with the critical left eigenvector eliminates nonresonant terms on the right-hand side; we get the well-known Ginzburg-Landau equation for the amplitude

$$\left(\frac{\partial}{\partial\tau_2}-V\frac{\partial}{\partial\xi_2}\right)A=\mu A+D\frac{\partial^2 A}{\partial\xi_1^2}+r|A|^2A. \tag{C29}$$

The bifurcation parameter is

$$\mu=\frac{(v_c|L^{(2)}u_c)}{(v_c|u_c)}. \tag{C30}$$

The linear terms (C26) and (C27) are combined in the diffusion coefficient

$$D=-\frac{1}{2}\frac{d^2\lambda}{dk^2}=\left(v_c\left|[L'(k_c)-iV1]\left(\frac{1}{L'(k_c)-i\omega_c 1}\right)_{\langle\nu_c\rangle}[L'(k_c)-iV1]u_c\right.\right)-\frac{1}{2}(v_c|L''(k_c)u_c) \tag{C31}$$

and the drift velocity (C19). The Hopf coefficient

$$r=\frac{(v_c|\tilde{\Gamma}+\Delta)}{(v_c|u_c)} \tag{C32}$$

has contributions from quadratic,

$$\tilde{\Gamma}=2\sum_{\alpha,\beta} e^{ik_c\alpha}C^{(\alpha\beta)}\{u_c,-2\Gamma_a\}+2\sum_{\alpha,\beta} e^{ik_c(2\beta-\alpha)}C^{(\alpha\beta)} \times\{u_c^*,-\Gamma_b\}, \tag{C33}$$

as well as from cubic terms

$$\Delta:=3\sum_{\alpha,\beta,\gamma} D^{(\alpha,\beta,\gamma)}\{u_c,u_c,u_c^*\}e^{ik_c(\alpha+\beta-\gamma)}. \tag{C34}$$

Using all symmetries of the system, the general expressions for the coefficients of the amplitude equation can be computed explicitly. If the system is inversion symmetrical, the drift velocity vanishes at $k_c=0$ and $k_c=\pi$. If the critical eigenvalue has a vanishing imaginary part (soft-mode), we obtain the real Ginzburg-Landau equation.

APPENDIX D

Parity breaking and parity preserving descriptions of 2-sublattice systems

For application to antiferromagnets, the perturbation theory of Appendix C has to be generalized to chains where the coupling induces alternating resting positions of the oscillators. The most simple approach describes two neighboring oscillators as one oscillator with twice as many degrees of freedom. This formal combination of pairs of oscillators however produces parity breaking terms that can lead to substantial complications and misinterpretations. In recent papers this basic symmetry problem led to differing long wavelength approximation of one and the same classical discrete spin chain described by the undamped Landau-Lifshitz equation

$$-\dot{\mathbf{S}}_i=J\mathbf{S}_i\times(\mathbf{S}_{i-1}+\mathbf{S}_{i+1}), \tag{D1}$$

where $J<0$ is a real coupling parameter. In the ground state of model (D1) with $J<0$, neighboring spins are aligned antiparallel. The spins belong alternately to two collinear sublattices. Skipping additional anisotropy and external field terms and scaling away differing signs and constants, we summarize the different continuum models of (D1) given in the literature. This limit is based on the hypothesis that, for excitations of the ground state, each sublattice can be described by slowly varying smooth functions.

The spin with the odd index $2n+1$ is described by the continuous field $\mathbf{S}_o(x)=\mathbf{S}_{2n+1}$ at the site $x=(2n+1)a$. The lattice constant a is small and the function $\mathbf{S}_o(x)$ is taken to be differentiable. The spins $\mathbf{S}_{2n},\mathbf{S}_{2n+2}$ correspond to the continuous field $\mathbf{S}_e$ at $x-a=2na$ and $x+a=(2n+2)a$, respectively. Introducing the vectors

$$\tilde{\mathbf{m}}=\frac{\mathbf{S}_o(x)+\mathbf{S}_e(x-a)}{2},$$

$$\mathbf{l}=\frac{\mathbf{S}_o(x)-\mathbf{S}_e(x-a)}{2}, \tag{D2}$$

and applying a second order Taylor expansion at $x-a=2na$ for $\mathbf{S}_{2n+2}=\mathbf{S}_e(x-a+2a)$ and an expansion at $x=(2n+1)a$ for $\mathbf{S}_{2n-1}=\mathbf{S}_o(x-2a)$ one gets

$$-\dot{\mathbf{l}}=4J\mathbf{l}\times\tilde{\mathbf{m}}+2Ja(\tilde{\mathbf{m}}\times\tilde{\mathbf{m}}_x-\mathbf{l}\times\mathbf{l}_x) +2Ja^2(\mathbf{l}\times\tilde{\mathbf{m}}_{xx}+\mathbf{l}_{xx}\times\tilde{\mathbf{m}}),$$

$$-\dot{\tilde{\mathbf{m}}}=2Ja(\mathbf{l}\times\tilde{\mathbf{m}})_x+2Ja^2(\tilde{\mathbf{m}}\times\tilde{\mathbf{m}}_{xx}+\mathbf{l}_{xx}\times\mathbf{l}). \tag{D3}$$

Rescaling the time with $-2Ja$ and setting $\mathbf{m}=\tilde{\mathbf{m}}/a$ one finds in the leading order [15,16]

$$\dot{\mathbf{l}}=2\mathbf{l}\times\mathbf{m}-\mathbf{l}\times\frac{\partial\mathbf{l}}{\partial x},$$

$$\dot{\mathbf{m}}=\frac{\partial}{\partial x}(\mathbf{l}\times\mathbf{m})-\mathbf{l}\times\frac{\partial^2}{\partial x^2}\mathbf{l}. \tag{D4}$$

Instead of combining $\mathbf{S}_o(x)$ at the site $2n+1$ with its left neighbor $\mathbf{S}_e(x-a)$ at $2n$ in definition (D2), one could equally choose its right neighbor $\mathbf{S}_e(x+a)$ at site $2n+2$. One would then get a set of equations equivalent to Eq. (D4), in which the first spatial derivatives have opposite sign. This formal ambiguity leads to contradictory results [16], if nonzero values of $\mathbf{m}$ are interpreted as an indication of a local magnetization [15]. Therefore no physical conclusions should be drawn from the presence of the first spatial derivatives.

This ambiguity is avoided by the parity preserving definition

$$\mathbf{M}=\frac{\mathbf{S}_o(x)+\mathbf{S}_e(x)}{2a},$$

$$\mathbf{L}=\frac{\mathbf{S}_o(x)-\mathbf{S}_e(x)}{2}, \tag{D5}$$

using an expansion of the continuous field $\mathbf{S}_e(x)$ at $x=(2n+1)a$ to obtain $\mathbf{S}_{2n/2n+2}$. One obtains [9]

$$\dot{\mathbf{L}}=2\mathbf{L}\times\mathbf{M},$$

$$\dot{\mathbf{M}}=-\frac{1}{2}\mathbf{L}\times\frac{\partial^2}{\partial x^2}\mathbf{L}. \tag{D6}$$

The sets (D6) and (D4) are equivalent; they are linked to each other by the transformation

$$\mathbf{m}=\mathbf{M}+\frac{1}{2}\mathbf{L}_x,$$

$$\mathbf{l}=\mathbf{L}. \tag{D7}$$

Consequently, Eqs. (D6) have the symmetry of the original system while the symmetry breaking terms of the macro-

scopic equations (D4) are nothing but an avoidable complication. Macroscopically, finite values of **M** or **m** both correspond to zero magnetizations.

For the continuum description [17,18]

$$\dot{\mathbf{l}} = -\mathbf{l} \times \frac{\partial \mathbf{l}}{\partial x}, \tag{D8}$$

it is assumed that **m** is small. However, there is no reason for this assumption because **m** is driven by the term $\mathbf{l} \times (\partial^2/\partial x^2)\mathbf{l}$. This approximation neglects all terms, retaining only the one that may be eliminated exactly by transformation (D7). Consequently, Eq. (D8) is not equivalent to correct continuum limits (D6),(D4).

We will now transfer the formalism described in Appendix C to chains with two (or more) types of coupled oscillators on alternating lattice sites retaining the inversion symmetry. To obtain a formulation analogous to Eq. (D5), we start with a general chain of identical oscillators ϕ_n with next-neighbor coupling

$$\dot{\phi}_n = F(\phi_n, \phi_{n-1}, \phi_{n+1}). \tag{D9}$$

Decomposing the vectors ϕ in upper and lower parts as

$$\phi_n = \begin{pmatrix} \alpha_n \\ \beta_n \end{pmatrix} \tag{D10}$$

and specializing the general coupling function F so as to yield

$$\begin{pmatrix} \dot{\alpha}_n \\ \dot{\beta}_n \end{pmatrix} = \begin{pmatrix} G(\alpha_n, \beta_{n+1}, \beta_{n-1}) \\ H(\beta_n, \alpha_{n+1}, \alpha_{n-1}) \end{pmatrix} \tag{D11}$$

for the equation of motion, (D10) divides ϕ in two kinds of oscillators α and β. The specific choice of F guarantees that α oscillators interact only with β oscillators on adjacent sites and vice versa. Consequently, the chain of ϕ oscillators is decomposed in two mutually independent identical chains with alternating oscillators α and β. These chains are governed by the same amplitude equation as the original ϕ-chain.

Conversely one can derive the amplitude equation for any chain of two alternating oscillators $(\ldots, \beta_{n-1}, \alpha_n, \beta_{n+1}, \alpha_{n+2}, \ldots)$ by combining the two types of oscillators α_n and β_n to a single ''superoscillator'' ϕ_n (D10). This chain has the form (D11) or (D9). The formalism of one-oscillator chains can now be applied.

The antiferromagnetic spin chain described in the text is an example of a two-oscillator chain because the spin oscillators of the two sublattices are influenced by different effective fields. It can be reduced to a one-oscillator chain before the amplitude equation is derived.

[1] N. Bloembergen and R. W. Damon, Phys. Rev. **85**, 699 (1952); N. Bloembergen and S. Wang, *ibid.* **93**, 72 (1954).

[2] H. Suhl, J. Phys. Chem. Solids **1**, 209 (1957).

[3] H. Benner, F. Rödelsperger, and G. Wiese, in *Nonlinear Dynamics in Solids*, edited by H. Thomas (Springer-Verlag, Berlin, 1992), pp. 129–155; C. D. Jeffries, P. H. Bryant, K. Nakamura, J. Appl. Phys. **64**, 5382 (1988); M. Warden and F. Waldner, J. Appl. Phys. **64**, 5386 (1988); B. Rumpf and H. Sauermann, Phys. Lett. A **185**, 461 (1994).

[4] V. E. Zakharov, V. S. L'vov, and S. S. Starobinets, Usp. Fiz. Nauk **114**, 609 (1974) [Sov. Phys. Usp. **17**, 896 (1975)].

[5] X. Y. Zhang and H. Suhl, Phys. Rev. Lett. **57**, 1480 (1986).

[6] F. J. Elmer, Physica D **30**, 321 (1988); F. Matthäus and H. Sauermann, Z. Phys. B **99**, 611 (1996).

[7] F. J. Elmer, Phys. Rev. B **53**, 14 323 (1996).

[8] H. J. Mikeska and M. Steiner, Adv. Phys. **40**, 191 (1991); G. Srinivasan and A. N. Slavin, *High Frequency Processes in Magnetic Materials*, (World Scientific, New York, 1995); H. J. Mikeska and H. Benner, in *Nonlinear Dynamics in Solids* (Ref. [3]), p. 156–193; A. N. Slavin, IEEE Trans. Magn. **31**, 3461 (1995); B. Rumpf, Phys. Lett. A **221**, 197 (1996).

[9] A. M. Kosevich, B. A. Ivanov, and A. S. Kovalev, Phys. Rep. **194**, 117 (1990).

[10] V. G. Bar'yakhtar, M. V. Chetkin, B. A. Ivanov, and S. N. Gadetskii, *Dynamics of Topological Solitons* (Springer-Verlag, Berlin, 1994).

[11] K. Gnatzig, H. Dötsch, M. Ye, and A. Brockmeyer, J. Appl. Phys. **62**, 4839 (1987).

[12] D. A. Garanin, Physica A **172**, 470 (1991); T. Plefka, Z. Phys. B **90**, 447 (1993).

[13] G. F. Herrmann, Phys. Rev. **133**, 1334 (1964).

[14] A. I. Akhiezer, V. G. Bar'yakhtar, and S. V. Peletminskii, *Spin Waves* (North-Holland, Amsterdam, 1968).

[15] N. Papanicolaou, Phys. Rev. B **51**, 15 062 (1995).

[16] N. Papanicolaou, Phys. Rev. B **55**, 12 290 (1997).

[17] M. Daniel and A. R. Bishop, Phys. Lett. A **162**, 162 (1992).

[18] R. Balakrishnan, A. R. Bishop, and R. Dandoloff, Phys. Rev. B **47**, 3108 (1993).

[19] J. Guckenheimer and P. Holmes, *Nonlinear Oscillations, Dynamical Systems, and Bifurcations of Vector Fields* (Springer-Verlag, New York, 1983).

[20] M. C. Cross and P. C. Hohenberg, Rev. Mod. Phys. **65**, 851 (1993).

[21] W. van Saarloos and P. C. Hohenberg, Phys. Rev. D **56**, 303 (1992).

[22] S. Rakhmanova and D. L. Mills, Phys. Rev. B **54**, 9225 (1996).

[23] A. Riegert, Diplom-theses, Darmstadt 1995.

[24] Y. Kuramoto and T. Yamada, Prog. Theor. Phys. **56**, 679 (1976); T. Yamada and Y. Kuramoto, *ibid.* **56**, 681 (1976).

[25] A. C. Newell and Y. Pomeau, J. Phys. A **26**, L429 (1993).

[26] A. C. Newell and J. A. Whitehead, J. Fluid Mech. **38**, 279 (1969).

[27] Y. Kuramoto and T. Tsuzuki, Prog. Theor. Phys. **54**, 687 (1975); A. Wunderlin and H. Haken, Z. Phys. B **21**, 393 (1975); H. Haken, *Synergetics* (Springer-Verlag, Berlin, 1977).

[28] W. Just (unpublished).